A prototype PVDF underwater pressure-gradient acoustic intensity probe

Damien Killeen (1, 2), Matthew Legg (1) and David Matthews (1, 2)

(1) Maritime Operations Division, Defence Science and Technology Organisation, WA, Australia.
(2) Department of Applied Physics, Curtin University, WA, Australia.

ABSTRACT

This paper reports on a prototype underwater pressure-gradient intensity probe consisting of two parallel PVDF films separated by a thin, rigid plate and potted in polyurethane. Field tests were conducted to measure the acoustic intensity produced by a single source transmitting narrow and broadband signals. Data was recorded from both PVDF elements simultaneously as the probe was rotated. Acoustic intensity was estimated by applying a set of signal processing techniques to the recorded data. The results indicate that the probe can be used to estimate one-dimensional acoustic intensity at ultrasonic frequencies. Details of the signal processing methods and results from the field test will be presented.

INTRODUCTION

Acoustic intensity probes measure the acoustic intensity vector's magnitude and direction. Intensity is defined as energy flux density, and it is readily shown that (Fahy, 1989)

$$\mathbf{I}_i(t) = p(t)\mathbf{u}(t) \tag{1}$$

where $\mathbf{I}_i$ is the instantaneous acoustic intensity vector, t is time, p is the acoustic pressure and $\mathbf{u}$ is the fluid-particle acoustic velocity vector.

Direct measurement of fluid-particle acoustic velocity has been demonstrated underwater where neutral buoyancy of the probe can be achieved (Leslie et al., 1956). However, transduction of probe motion requires high sensitivity and very low noise characteristics of its inertial sensor. While this has been overcome through the use of single crystal piezoelectric accelerometers (Shipps and Deng, 2003), these devices are not readily available in Australia. Combining pressure and inertial sensors in a single probe to measure intensity underwater has previously been demonstrated (Gabrielson et al., 1995).

In linear acoustics, the application of Newton's second law, under uniform flow conditions, results in the linear fluid momentum equation (Kinsler et al., 1950):

$$-\nabla p(t) \cong \rho \frac{\partial \mathbf{u}}{\partial t} \tag{2}$$

where ρ is the fluid density at equilibrium and ∇ is the spatial gradient operator. Substitution of (2) into (1) gives

$$\mathbf{I}_i(t) \cong -\frac{p(t)}{\rho}\int_{-\infty}^{t} \nabla p(\tau)\, d\tau\,. \tag{3}$$

For two pressure sensors p_1 and p_2 separated by the vector $\mathbf{n}$, p can be approximated by their average. The finite-difference approximation of the pressure gradient from p_1 to p_2 is their difference scaled by n, the magnitude of $\mathbf{n}$. Thus the component of instantaneous intensity in the direction of $\mathbf{n}$ is approximately

$$I_n(t) \cong \frac{p_1(t)+p_2(t)}{2\rho n}\int_{-\infty}^{t}\left[p_1(\tau)-p_2(\tau)\right]d\tau\,. \tag{4}$$

Pressure-gradient intensity probes based on this principle have been used extensively in air acoustics, where direct measurement of acoustic intensity has only relatively recently become possible (de Bree et al., 1996). An underwater pressure gradient probe using PVDF sensors was considered by Segota (1990) and a PVDF-bimorph underwater acoustic fluid-particle velocity sensor has been proposed by Josserand and Maerfeld (1985).

An advantage of pressure-gradient intensity probes over inertial-type probes is that they only require calibration of their pressure transducers, for which there are many resources available. A disadvantage is that sensor phase mismatch produces erroneous intensity measurements in all acoustic fields. Sensor phase mismatch in inertial-type probes is only problematic in highly reactive fields (Jacobsen and de Bree, 2005) where the energy transfer is largely oscillatory and not associated with a net energy transport. The errors associated with the finite difference approximation are another disadvantage of pressure-gradient intensity probes.

This paper describes the fabrication and testing of a simple, low-cost, underwater intensity probe, based on the above principle, using two PVDF films.

MEASUREMENT METHOD

Probe fabrication

The probe has two polyvinylidine fluoride (PVDF) piezoelectric film elements from Measurement Specialties. The specific film used was DT1-028K/L. These rectangular films (41 mm by 16 mm) have screen printed silver electrodes on either side. The film thickness is 28 μm and has a capacitance of 1.38 nF. The PVDF films were attached using contact adhesive to either side of a 1.6 mm thick fibreglass plate as shown in Figure 1. The negative side of each film was placed onto the fibreglass.

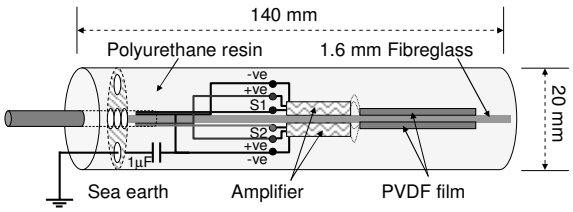

Figure 1. PVDF pressure gradient intensity probe.

The film outputs were connected to pre-amplifiers with ~30 dB of gain. In order to minimize 50 Hz noise the cable shielding was coupled to the sea via a 1 μF capacitor. The entire sensor configuration was then encapsulated in Robnor polyurethane resin (EL171C). This resulted in a sensor 140 mm long with a diameter of 20 mm.

Field trial

The probe was positioned between two HTI-96-MIN series hydrophones, as shown in Figure 2, which were used to determine the probe's orientation to the source. All three sensors were pointing downwards. The HTI hydrophones have built in pre-amplifiers to give a nominal sensitivity of -165 dB re 1 V/μPa up to 30 kHz. Additional substitution sensitivity measurements were conducted up to 96 kHz and are discussed below.

The three sensors were secured through a piece of 20 mm diameter PVC pipe such that the probe was 0.25 m from each HTI hydrophone. A weight was suspended directly below the probe at a distance of 1.18 m to stabilise the structure. The probe was positioned such that the PVDF films were perpendicular to the length of PVC pipe. The entire rig was then suspended off a pontoon into salt water at a depth of 4.4 m. The rig was rotated manually from the surface, by a few turns in each direction. The water depth at the receivers and transmitter was 10.2 m and 10.7 m respectively. Sea surface roughness was zero and the air temperature reached 29.5° C.

An ITC 1032 hydrophone was used as a transmitter positioned 11.6 m from the probe also at a depth of 4.4 m. The transmitted signals were generated in Matlab and saved as WAV files. These files were then replayed by a Fostex FR-2 portable 2 track memory recorder, through a Marantz power amplifier connected to the ITC 1032 via an impedance matching transformer.

The signals consisted of pseudorandom Gaussian noise, bandpass filtered with a passband region of 24 to 44 kHz with over 50 dB stopband attenuation. A single tone was added to this noise at 2, 5, 10, 15 or 20 kHz to produce five separate signal files. The intention was to use the broadband noise received by the HTI hydrophones to determine the orientation of the rig, and to use the tones to measure sensitivity, directionality and intensity.

The outputs from the two HTI hydrophones and the two-channel probe were recorded simultaneously using an Edirol/Roland R-4PRO 4 channel recorder. All channels were recorded using a sampling rate of 96 kHz. Once the ITC 1032 was transmitting the receiver rig was slowly rotated while collecting data for 10 minutes.

Sensitivity estimation

Standard calibration methods for pressure gradient probes (Fahy, 1989) are not readily reproducible for the geometry of this probe, as it is necessary to calibrate the sensors after encapsulation. For the purposes of this paper, only a confidence check was required, for which field measurements of sensitivity are sufficient.

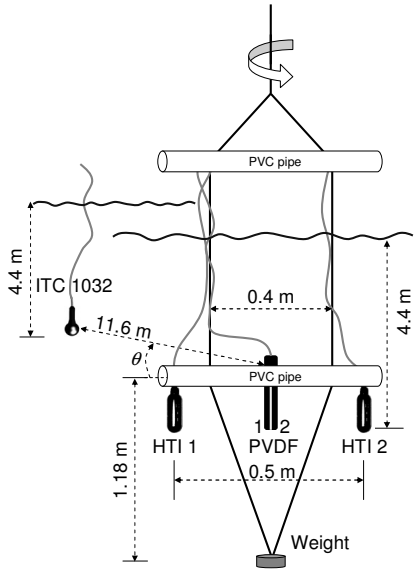

Figure 2. Rotating rig used to test the intensity probe.

The PVDF sensitivity was measured by comparing voltage levels produced by the HTI and PVDF sensors during the trial. As a verification exercise these sensors were used to estimate the source level of the ITC 1032, and this was compared with independent measurements of the transmit sensitivity of the ITC 1032, conducted at a later date.

To measure the transmit sensitivity of the ITC 1032 transducer a Reson TC 4014-5 hydrophone was positioned 1 m away during transmission of the same signals as in the field trial, using the same equipment and settings, on a day with nearly identical environmental conditions. The setup is shown in Figure 3. The transmitter was lowered to a depth of 4 m and the received signals were recorded on a Fostex FR-2 portable 2 track memory recorder via a Reson TC 4014-5 hydrophone. The TC 4014-5 is a broad band (15 Hz – 480 kHz) spherical, omnidirectional hydrophone with a built-in, low-noise 26 dB pre-amplifier.

The HTI hydrophones' sensitivities are nominally rated up to 30 kHz. As the frequencies used in this trial extend to 48 kHz, measurement of the HTI sensitivity was required. The HTI sensitivities were measured by substitution with the Reson TC 4014-5 using the rig shown in Figure 4. Ambient noise was recorded on an R-4PRO, sampled at 192 kHz. Two-channel recordings were conducted for each HTI individually alongside the TC 4014-5 allowing the highest sample rate on the R-4PRO. The hydrophone rig was located midwater in a 10.4 m water column. This measurement was conducted several days after the ITC 1032 transmit sensitivity was measured.

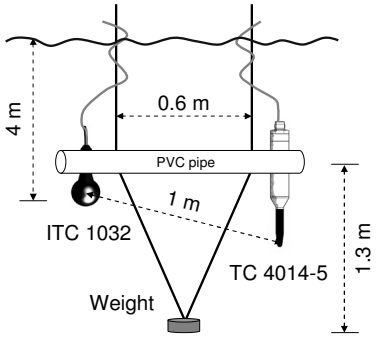

Figure 3. ITC 1032 transmit sensitivity measurement rig.

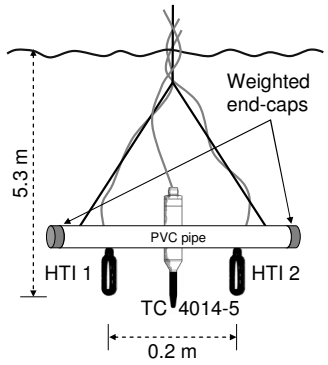

Figure 4. Rig used to measure HTI sensitivity by substitution with the Reson TC 4014-5.

RESULTS

Rig orientation

The orientation of the rotating rig was computed using the time delay of arrival of the transmitted signal between each of the HTI hydrophones. A maximum likelihood time delay estimator derived for Gaussian signal and uncorrelated Gaussian noise (Knapp and Carter, 1976) was used by selecting the time delay Δt to maximise the cross-correlation $R(\Delta t)$ given by

$$R_{x,y}^{(ML)}(\Delta t) = \int_{-\infty}^{\infty} \psi_{ML}(f) G_{x,y}(f) e^{i2\pi f \Delta t} df \tag{5}$$

where $G_{x,y}(f)$ is the cross-spectral density of time series x and y at frequency f, and

$$\psi_{ML}(f) = \frac{1}{\left|G_{x,y}(f)\right|} \frac{\left|\gamma_{x,y}(f)\right|^2}{\left(1-\left|\gamma_{x,y}(f)\right|^2\right)} \tag{6}$$

in which $\gamma_{x,y}(f)$ is the mean-square coherence of time series x and y.

The rig orientation was computed from the estimated time delays by the far field assumption that:

$$\theta = \cos^{-1}\left(\frac{c\Delta t}{d}\right) \tag{7}$$

where θ is the angle from the rig orientation to the source direction (Figure 2), c is the speed of sound in water and d the distance between the HTI hydrophones.

This angle is conically ambiguous, however as the source and receivers were in the same horizontal plane, this reduces to a left-right ambiguity which was resolved by recording the observed orientation angle of the rig throughout the trial.

Short time-scale errors (variance around the running mean) in this method of angle estimation are caused by variance in the time delay estimates (Ferguson, 2000) which is determined by the correlation properties of the signal and the noise present, and their signal-to-noise ratio. The relationship between the angle and time delay variance is (Carter, 1981)

$$\sigma_{\theta'-\theta}^2 = \frac{c^2 \sigma_{\Delta t'-\Delta t}^2}{d^2 \sin^2\theta} \tag{8}$$

where $\sigma^2_{\theta'-\theta}$ and $\sigma^2_{\Delta t'-\Delta t}$ are the short time-scale variance of the bearing and time-delay estimates, respectively.

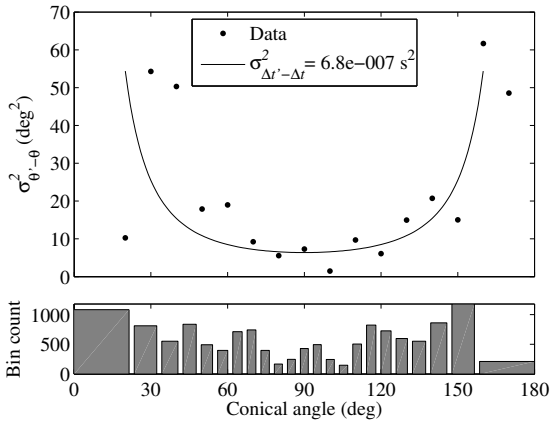

Figure 5. Bearing estimation variance (top) fitted by equation (8), and the resulting bearing bins with the frequency of occurrence in each (bottom).

The data for each run of the field trial was high pass filtered with a 24 kHz cut off, then segmented into 0.17 s frames. The time delay for each frame was estimated with equation (5). Frames where the correlation was less than 0.5 or the time delays exceeded $\pm d/c$ were discarded (the sound speed was estimated at 1530 ms^{-1}, due to the warm, still conditions). The first 15 s of the first run were also discarded as the rig was spinning too quickly. The remaining delays were converted into angles with equation (7) and these were smoothed with a moving average boxcar window of length 1.4 s. This window length was arbitrarily chosen to be eight frames long; roughly the length of time taken for the rig to turn 1°. Several outliers were also removed where strong correlations were found at time delays within $\pm d/c$, likely caused by snapping shrimp. These were identified when $\theta' - \theta > 3\sigma_{\theta'-\theta}$.

The variance of the estimated angles about their moving average was computed for all five runs, and the average estimated angle variance in smoothed angle bins 10° wide computed (Figure 5, top, dots). Equation (8) was fitted to the result (solid line), and used to define a series of azimuth bins. The fit corresponds to an uncertainty in the time delay estimates of ±0.5 samples. Each bin is two standard deviations wide, starting with a bin centred at 90°. The smoothed angles were then used to determine the azimuth bin that each data frame belonged to.

Probe directionality

The directionality of each individual PVDF sensor, and the 'virtual' sensor formed by their average, was estimated. The HTI hydrophones were used as a reference because they were simultaneously sampled with the intensity probe and are known to be omnidirectional in the horizontal plane.

Tonals included in the transmitted signals were originally intended for estimation of the pressure directionality and sensitivity at those frequencies, however strong interference from the surface reflected signal precluded their use for this purpose. Instead, broadband processing of the Gaussian signal in the upper half of the band, between 26 kHz and 42 kHz, was used because the coherent effects of propagation loss are removed and incoherent propagation models could be employed with much greater confidence.

To estimate each sensor's directionality, the high-pass filtered data was segmented into frames 8192 samples (0.0853 s) long and the variance of each frame used as an estimate of their mean-square level. These levels were binned according to the previously computed azimuth for the frame. The mean and variance of the mean-square levels in each azimuth bin

were then estimated. The results are shown in Figure 6 (PVDF) and Figure 7 (HTI), normalised to a maximum of 0 dB.

The PVDF sensors' results in Figure 6 display a moderate directionality that is maximal 45° off the normal to the film. Normal incidence is around -1 dB on the exposed side and -3 to -5 dB on the side glued to the fibreglass plate. The results for the HTI hydrophones shown in Figure 7 were expected to be omnidirectional; however a 6 dB deep, 90° wide null is evident for both sensors. In both cases the orientation of the null is towards the other sensor, along the axis of the rig, thus is likely due to acoustic shadowing. The line-of-sight shadow region on the HTI hydrophones due to the probe is only 10° wide, discounting it as the sole cause. Another cause could be the PVC pipe obstructing the surface bounce.

Probe sensitivity

The HTI hydrophones' sensitivities were estimated by substitution with the Reson TC 4014-5 calibrated reference hydrophone, in the rig shown in Figure 4. After configuring the R-4PRO recorder to ensure ambient noise levels did not clip its input, two-channel recordings were made of first HTI-1 with the Reson, then HTI-2. Afterwards, recordings were made of a Neutric Minirator MR1 outputting -34 dBV white noise into each R-4PRO channel. The Neutric recordings were used to calibrate the R-4PRO input gain for each channel, in volts per quanta. This gain was applied to the ambient noise recordings, and power spectral densities in V^2Hz^{-1} for both HTI hydrophones and the Reson were computed.

The Reson's known sensitivity was used to convert its power spectral density into μPa^2Hz^{-1}. By making the broad assumption that the sound pressure level at the HTI was the same as that at the Reson, the sensitivity of the HTI was estimated as the ratio between the HTI voltage level and the sound pressure level at the Reson. This was computed in one-third octave bins and the relevant frequency range is shown at the top of Figure 8. To estimate the sensitivity of the PVDF sensors, their voltage levels were compared to those of the HTI hydrophones when the rotating rig was at specific orientations. The azimuth of maximum response was used for the PVDF sensors, being ~35° and ~145° for PVDF-1 and PVDF-2, respectively. For comparison with the HTI hydrophones it was necessary to choose an azimuth where the range to the source was the same for both the HTI and PVDF sensors. The range to the HTI-1 and PVDF-1 sensors was equal at 88.8° and to HTI-2 and PVDF-2 at 91.2°, both of which were most closely represented by the 90° azimuth bin.

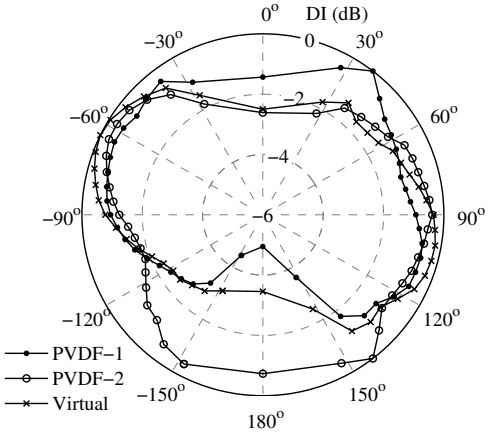

Figure 6. Directionality of the PVDF sensors and the 'Virtual' sensor formed by their average. Typical uncertainty bounds are ±1.5 dB.

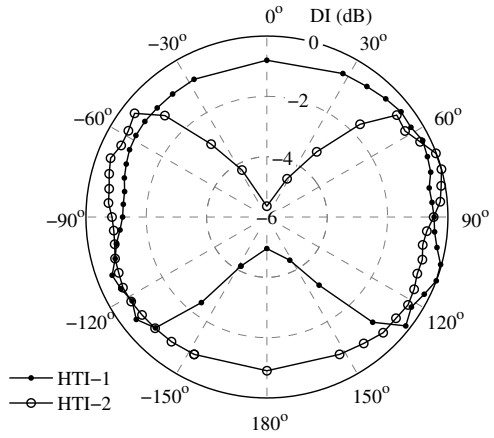

Figure 7. Directionality of the HTI sensors. Typical uncertainty bounds are ±1.5 dB.

The directivity index of the HTI hydrophones at this azimuth was considered to be 0 dB. Once again, recordings of the Neutric were made to determine the R-4PRO channel gains. Gain corrections were applied and power spectral densities in V^2Hz^{-1} produced. The HTI power spectral densities were converted to μPa^2Hz^{-1} using their estimated sensitivities. The spectra were smoothed by a moving average filter 517 Hz wide (the observed interference-pattern null separation). The sensitivity of PVDF-1 and PVDF-2 were then determined by the ratio of their voltage levels to the average of the sound pressure levels at HTI-1 and HTI-2. The results are shown at bottom of Figure 8.

To verify the HTI and PVDF sensitivities, they were used to estimate the source level of the ITC 1032 by removing 11.6 m of semi-spherical spreading loss. Modelling the sea surface as perfectly reflective and the bottom as non-reflective, the surface area over which the sound power spread was that of an 11.6 m radius sphere truncated 4.4 m above its centre. This produced 19.7 dB of spreading loss.

The source level of the ITC 1032 was measured by placing the Reson TC 4014-5 calibrated reference hydrophone 1 m from the ITC 1032 (Figure 3) while it transmitted the same signals with an identical equipment set up as in the field trial. The Reson signal was recorded on a Fostex recorder, the input gain of which was again determined by recording the output of the Neutric. The source level estimated by the HTI hydrophones and PVDF sensors are compared to that measured by the Reson in Figure 9 and the agreement is considered good (within ±3 dB) given the methodology.

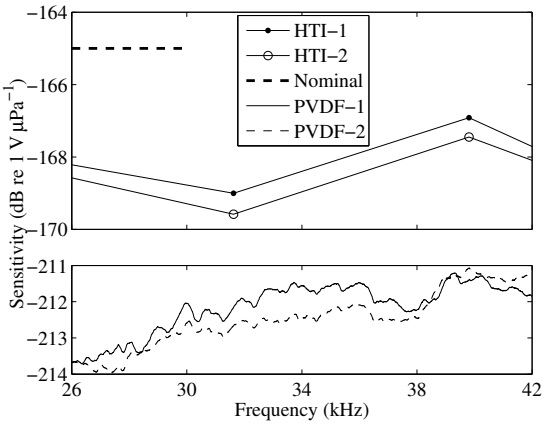

Figure 8. Measured sensitivity of the HTI and PVDF sensors and nominal HTI sensitivity.

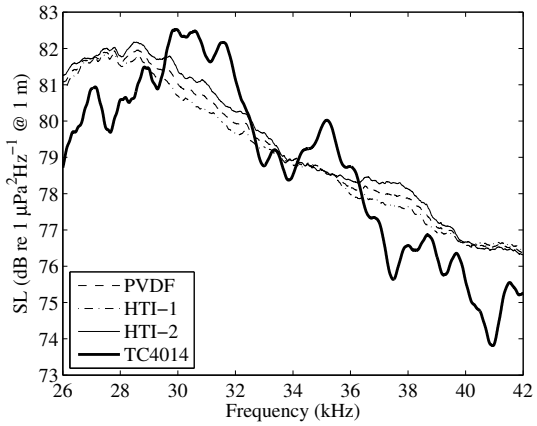

Figure 9. Source level of the ITC 1032 estimated from the PVDF and HTI sensors, and measured by the TC 4014-5.

Intensity estimates

The magnitude of active acoustic intensity is often approximated by

$$I_{FF} = \frac{p^2}{\rho c} \tag{9}$$

where the far-field, free-field and harmonic source assumption has been made that the acoustic impedance is ρc. Alternatively, the time-average of equation (4), denoted $\langle I_n \rangle_t$, can be used to estimate the component of active intensity in the direction of **n**. Both of these estimation methods were investigated. The data was segmented into 8192 sample (0.0853 s) long frames and converted to omnidirectional pressure using the PVDF sensitivity and directionality determined in the previous section. The virtual sensor formed by the average of the two PVDF sensor's output was used for p in equation (9). The active intensity estimates using both methods are shown in Figure 10.

DISCUSSION

Figure 10 shows that equation (9) results in a perfectly directionless estimate of intensity, as can be expected from a scalar expression. This demonstrates that the PVDF film's directionality has been appropriately accounted for.

The pressure gradient intensity estimate shows a significant null (up to 20 dB) rotated away from the expected ±90°. Such a rotation could be produced by a phase mismatch between the PVDF sensors, as null rotation and phase mismatch are related by (Fahy, 1989)

$$\sin\left(\phi_r\right) = -\frac{\phi_s}{kn} \tag{10}$$

where ϕ_r is the null rotation angle, ϕ_s is the phase mismatch and k the wavenumber. For a small phase mismatch, the error in the intensity measurement is such that (Jacobsen, 1990)

$$\begin{aligned} \left\langle I_n \right\rangle_t &= I_a - \frac{\phi_s}{kn}\frac{p^2}{\rho c} \\ &= I_s \cos\left(\theta - \phi_r\right) + \sin\left(\phi_r\right)\frac{p^2}{\rho c} \end{aligned} \tag{11}$$

where I_s is the active intensity coming from the source and I_a is the component of I_s in the direction **n.**

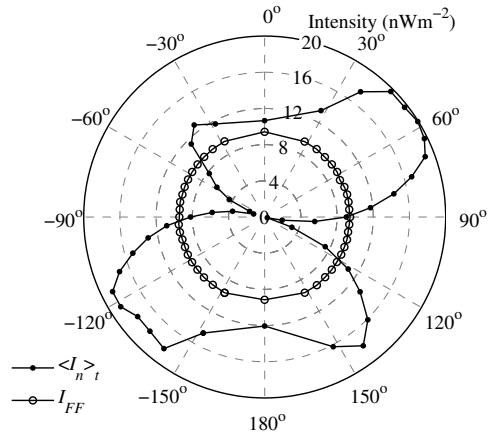

Figure 10. Active intensity computed by the pressure gradient technique ($\langle I_n \rangle_t$) and $p^2/\rho c$ (I_{FF}).

A fit of equation (11) to the data is shown in Figure 11 as a solid line. This indicates that phase mismatch is a possible cause of the rotation of the nulls; however misalignment of the probe in the rig will also be a contributing (or perhaps mitigating) factor. The fit was made with I_s = 32 nWm^{-2} and ϕ_r = 15°, which according to equation (10) indicates a phase mismatch of -0.06 radians at 34 kHz (mid-band). As the probe has no vertical directionality, the sound power of the source cannot be estimated due to the reverberation from the sea surface. It should be noted that the fitted value for I_s from the pressure-gradient measurements is over 3 times larger than the 9.4 nWm^{-2} estimate of I_{FF} from Figure 10.

Figure 11 also indicates a severe truncation of the dipole lobes within ±45° of their peak. Neither phase mismatch nor finite difference approximation errors explain this effect. The most likely cause of the effect is diffraction. Diffraction effects are identified by comparing the measured phase difference between the sensors to that expected in a free field at the points occupied by the sensors, such as in Krishnappa (1984). However, interference from the surface bounce and other propagation paths complicate this comparison significantly.

Resolving the source of the dipole lobe truncation will form further work. It is worth noting, however, that the arcs affected correspond to the shadow region displayed by the HTI hydrophones in Figure 7. A common cause consistent with these observations could be the PVC pipe obstructing the surface reflected acoustic energy.

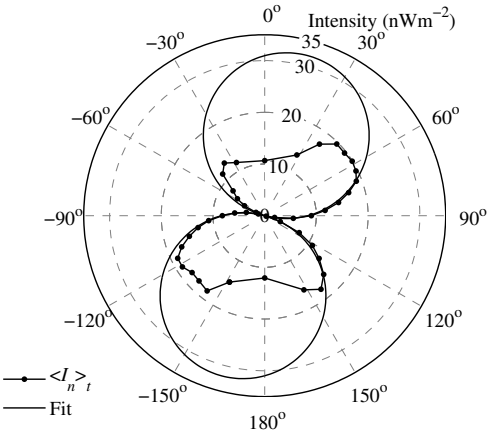

Figure 11. Active intensity measured by the pressure gradient probe ($\langle I_n \rangle_t$) fitted by equation (11).

CONCLUSIONS

A one-dimensional pressure-gradient acoustic intensity vector probe was constructed using two PVDF films and tested at sea in a rotating rig with a single source in the far field.

The sensitivity and directionality of the PVDF sensors in the probe were determined, and used to estimate the source level of the broadband signal. These source level estimates agreed within ±3 dB with subsequent measurements made by a reference hydrophone placed 1 m from the source.

Strong interference effects precluded the use of narrow band signals between 2 kHz and 20 kHz for estimating acoustic intensity. Instead, incoherent processing techniques made use of a broadband signal transmitted between 26 kHz and 42 kHz. The broadband signals were also used to determine probe orientation.

Active (time-averaged) intensity was estimated using two methods. The first method used a standard assumption that the acoustic impedance was ρc. The result was omnidirectional and the value was underestimated. The second method used a pressure gradient technique. This method showed two nulls of up to 20 dB separated by 180°, demonstrating the probe's ability to sense acoustic intensity.

Rotation of the nulls by 15° was observed, which can be explained by a combination of phase mismatch between the PVDF sensors and misalignment of the probe within the mounting rig.

A truncation of the expected dipole response was observed. This is unexplained, though is likely to be a diffraction issue related to the probe suspension rig. Further work is required to identify the cause.

ACKNOWLEDGEMENTS

The authors are grateful to Paul Kelly of CAS WA for supplying the pre-amplifiers used in the PVDF pressure gradient probe.

REFERENCES

CARTER, G. (1981) Time delay estimation for passive sonar signal processing. *Acoustics, Speech and Signal Processing, IEEE Transactions on,* 29**,** 463-470.

DE BREE, H.-E., LEUSSINK, P., KORTHORST, T., JANSEN, H., LAMMERINK, T. S. J. & ELWENSPOEK, M. (1996) The [mu]-flown: a novel device for measuring acoustic flows. *Sensors and Actuators A: Physical,* 54**,** 552-557.

FAHY, F. J. (1989) *Sound Intensity,* London, E & FN Spon.

FERGUSON, B. G. (2000) Variability in the passive ranging of acoustic sources in air using a wavefront curvature technique. *The Journal of the Acoustical Society of America,* 108**,** 1535-1544.

GABRIELSON, T. B., GARDNER, D. L. & GARRETT, S. L. (1995) A simple neutrally buoyant sensor for direct measurement of particle velocity and intensity in water. *The Journal of the Acoustical Society of America,* 97**,** 2227-2237.

JACOBSEN, F. (1990) Sound Field Indicators: Useful Tools. *Noise Control Engineering Journal,* 35**,** 37-46.

JACOBSEN, F. & DE BREE, H.-E. (2005) A comparison of two different sound intensity measurement principles. *The Journal of the Acoustical Society of America,* 118**,** 1510-1517.

JOSSERAND, M. A. & MAERFELD, C. (1985) PVF2 velocity hydrophones. *The Journal of the Acoustical Society of America,* 78**,** 861-867.

KINSLER, L. E., FREY, A. R., COPPENS, A. B. & SANDERS, J. V. (1950) *Fundamentals of Acoustics,* New York, John Wiley & Sons, Inc.

KNAPP, C. & CARTER, G. (1976) The generalized correlation method for estimation of time delay. *Acoustics, Speech and Signal Processing, IEEE Transactions on,* 24**,** 320-327.

KRISHNAPPA, G. (1984) Scattering/Diffraction Effects in the Two-Microphone Technique of Measuring Sound Intensity at Sound Incidence Angles Other than 0 degrees. *Noise Control Engineering Journal,* 22**,** 96-102.

LESLIE, C. B., KENDALL, J. M. & JONES, J. L. (1956) Hydrophone for Measuring Particle Velocity. *The Journal of the Acoustical Society of America,* 28**,** 711-715.

SEGOTA, J. P. (1990) The design, construction, and evaluation of a two-hydrophone intensity probe to determine the feasibility and limitations of underwater intensity, energy density, and impedance measurements. *Graduate Program in Acoustics.* The Pennsylvania State University.

SHIPPS, J. C. & DENG, K. (2003) A miniature vector sensor for line array applications. *OCEANS 2003. Proceedings.*